Gelatinization of Starch in Excess Water: Beyond the Melting of Lamellar Crystallites. A Combined Wide- and Small-Angle X-ray Scattering Study

Rudi Vermeylen,*,† Veerle Derycke,† Jan A. Delcour,† Bart Goderis,‡ Harry Reynaers,‡ and Michel H. J. Koch§

Laboratory of Food Chemistry, Katholieke Universiteit Leuven, Kasteelpark Arenberg 20, B-3001 Heverlee, Belgium, Molecular and Nanomaterials, Katholieke Universiteit Leuven, Celestijnenlaan 200F, B-3001 Heverlee, Belgium, and European Molecular Biology Laboratory, Hamburg Outstation, EMBL c/o DESY, Notkestrasse 85, D-22603 Hamburg, Germany

Received March 17, 2006; Revised Manuscript Received June 24, 2006

The gelatinization of waxy rice, regular rice, and potato starch suspensions (66% w/w moisture) was investigated by real-time small-angle X-ray scattering (SAXS) and wide-angle X-ray diffraction (WAXD) during heating and by fast ramp differential scanning calorimetry (DSC). The high-angle tail of the SAXS patterns suggested the transition from surface to mass fractal structures in the DSC gelatinization range. Amylose plays a major role in determining the dimensions of the self-similar structures that develop during this process as the characteristic power-law scattering behavior extends to lower scattering angles for regular than for waxy starches. Crystallinity of A-type starches is lost in the temperature region roughly corresponding to the DSC gelatinization range. At the end of the gelatinization endotherm, the B-type potato starch showed residual crystallinity (WAXD), while SAXS-patterns exhibited features of remaining lamellar stacks. Results indicate that the melting of amylopectin crystallites during gelatinization is accompanied by the (exothermic) formation of amorphous networks.

1. Introduction

Regular starch is a homopolysaccharide consisting of two types of α-D-glucose polymers, i.e., heavily branched amylopectin with a weight-average molecular weight (MW) of 0.7−57 × 10^8 and nearly linear amylose (MW 0.3−1.9 × 10^6).[1,2] In plant storage organs starch is laid down in water-insoluble granules. In wild-type starches, these granules contain typically 20−30% amylose, while waxy mutants essentially lack amylose. Granules display an onion-like organization with alternating amorphous and semicrystalline shells of 120−400 nm radial thickness.[3]

When hydrated, the semicrystalline shells are characterized by alternating high- and low-density lamellae with a repeat distance of 9−10 nm.[4] This feature has been attributed to the side-chain liquid-crystalline polymer (SCLCP) behavior of amylopectin.[5] Plasticization of amylopectin branch points (flexible spacers) would enable the double helices (mesogens) to be decoupled from the entropy maximizing polymer backbone. Consequently, double helices would align into lamellar register, resulting in a transition from the nematic to smectic phase. Amylopectin branching points are thus mainly clustered in the amorphous lamellae.[6,7] Moreover, double helices in the dense lamellae are packed in either a monoclinic or hexagonal crystalline unit cell, giving rise to A- or B-type diffraction patterns, respectively.[8]

When starch granules are suspended in sufficient water and heated to temperatures above 50−60 °C, the organization described above is destroyed by a process called gelatinization. The structural changes that take place during gelatinization include a simultaneous crystallite melting and double-helix unwinding,[9] absorption of water in the amorphous growth ring,[10] changes in shape and size of granules, dispersion of blocklet-like structures,[11] and leaching of amylose from the granules.[12] In this way, aqueous suspensions of discrete semicrystalline granules are transformed into a continuous amorphous gel phase. Changes in lamellar, crystalline, and double-helical order during the initial stages of gelatinization in excess water have been rationalized in terms of the SCLCP concept.[9] Classically, gelatinization is monitored with fast-ramp differential scanning calorimetry in which the endothermic event is associated with crystal melting[13] or double-helix unwinding.[14] Although recent low heating rate DSC[15] and high-pressure scanning transitiometry[16] studies suggest some exothermic amylopectin reassociations in the later stages of gelatinization, these molecular events have in general aroused little attention. The combined wide-angle X-ray diffraction (WAXD) and small-angle X-ray scattering (SAXS) study described below provides new information on this neglected aspect of starch gelatinization.

2. Experimental Section

2.1. Materials. Milled waxy (variety IR65) and regular (IR42) rices were obtained from the International Rice Research Institute (IRRI, Manilla, The Philippines). Potato tubers (Manon) were purchased from a local supermarket. Starch was isolated using a pronase-based procedure[17] with a previous Soxhlet rice kernel defatting step with chloroform/methanol (2:1 v/v).[18] After equilibration to the ambient air, moisture contents of the starches were 11.2% (IR65), 10.8% (IR42), and 14.5% (Manon).

2.2. Apparent Amylose. The apparent amylose contents of the starches were determined colorimetrically after defatting with aqueous

* To whom correspondence should be addressed. Phone: +32(0)16.32.16.34. Fax: +32(0)16.32.19.97. E-mail: rudi.vermeylen@scarlet.be.
† Laboratory of Food Chemistry, Katholieke Universiteit Leuven.
‡ Molecular and Nanomaterials, Katholieke Universiteit Leuven.
§ EMBL c/o DESY.

10.1021/bm060252d CCC: $33.50
Published on Web 08/10/2006

methanol (85% v/v) for 30 min at 60 °C.[19,20] Potato amylose (Calbiochem, Darmstadt, Germany) was used for calibration. Analyses were performed in triplicate with standard errors smaller than 5%.

2.3. Differential Scanning Calorimetry. DSC measurements were made on a Seiko DSC 120 (Kawasaki Kanagawa, Japan) using indium and tin as standards. Starch (5−6 mg dry weight) was accurately weighed into aluminum sample pans, and water was added directly to obtain a total moisture content of 66% w/w. Sample pans were hermetically sealed and heated at 2 °C/min from 20 to 110 °C with an empty pan as a reference. Onset (T_o), peak (T_p), and conclusion (T_c) temperatures of gelatinization were determined using Seiko software. At the end point of gelatinization (T_{end}) the heat flow returned to baseline level. Typical standard deviations from triplicate measurements were 0.1, 0.1, 0.3, and 1.0 °C for T_o, T_p, T_c, and T_{end}, respectively.

2.4. Temperature-Resolved X-ray Scattering. Temperature-resolved X-ray scattering experiments were performed on the X33 camera of the EMBL in HASYLAB on the storage ring DORIS III of the Deutsches Elektronen Synchrotron (DESY) in Hamburg (Germany) at a wavelength $\lambda = 0.15$ nm. SAXS and WAXD patterns of rice and potato starches were recorded with a standard data acquisition system with two delay line detectors in series.[21] Small-angle scattering data were collected in the angular range $0.03 < s < 0.35$ nm^{-1} [with $s = 2\sin(\theta)/\lambda$ the modulus of the scattering vector and 2θ = the scattering angle], as determined from calibration with dry calcified collagen. The WAXD pattern ($1.0 < s < 3.4$ nm^{-1}) was calibrated based on the position of sharp reflections of the potato starch specimen previously measured on a rotating anode wide-angle powder X-ray diffractometer calibrated with a silicon standard.[22]

Suspensions with a total moisture level of 66% were prepared by adding the required amount of deionized water directly to the starch. Samples were placed between two mica windows separated by a 1 mm thick brass spacer and inserted in a FP82HT hot stage (Mettler-Toledo, Zaventem, Belgium) through which the X-ray beam passed. After equilibration at 30 °C, suspensions were heated from 30 to 95 °C at a rate of 2 °C/min and recordings were binned in time frames of 30 s, corresponding to a resolution of one SAXS/WAXD pattern per 1 °C. The data were normalized with respect to the incident beam intensity, and correction was made for parasitic scattering by subtracting the scattering of an empty sample holder, taking into account the sample transmission.

2.5. WAXD Data Treatment. WAXD data processing, including normalization to equal total scattering in the measured angular range, was with the OTOKO software package.[23] Temperature dependence of the crystallinity index (CI) was quantified as explained earlier.[24]

2.6. SAXS Data Treatment. To determine structural characteristics of the alternating crystalline and amorphous lamellae, the constant scattering due to small-scale density fluctuations was subtracted using a modified Porod equation.[25,26] To that end, eq 1 was fitted to the high-angle tail of SAXS patterns (0.18−0.35 nm^{-1}) using the Marquardt−Levenberg nonlinear least-squares curve-fitting algorithm.

$$I(s) = B + \frac{C}{s^4}\exp(-2\pi E^2 s^2) \qquad (1)$$

Here B is the constant background, C the so-called Porod constant, and E the thickness of the transition layer between the crystalline and amorphous phases. For $E = 0$, eq 1 reduces to the classical Porod equation. Background-corrected intensities were converted to linear correlation functions ($K(x)$) by the Fourier cosine transformation

$$K(x) = \int (I(s) - B)s^2 \cos(2\pi xs)\mathrm{d}s \qquad (2)$$

The lamellar repeat distance (D) of the stacked lamellar structure was estimated directly from the position of the first side maximum of $K(x)$. The fractional lamellar crystallinity (φ) and the total scattering power, or invariant Q_{id}, of the corresponding ideal lamellar stacked system were obtained from analysis of the autocorrelation triangle.[26]

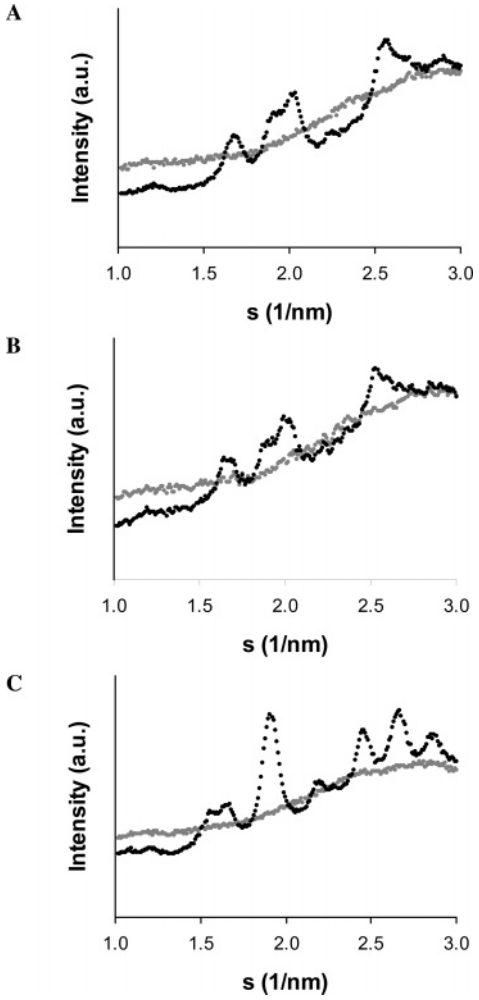

Figure 1. Wide-angle X-ray scattering patterns of waxy rice starch (A), regular rice starch (B), and potato starch (C) suspensions at 30 (black dots) and 95 °C (grey dots).

The scattering patterns from self-similar, fractal structures are described by eq 3

$$I(s) = B + Cs^{-d} \qquad (3)$$

The constant background scattering B is caused by density fluctuations with small dimensions compared to those of the fractal object. C is a scaling constant, and d is the power-law exponent, which expresses the fractal dimension of the surface/mass fractal structure. Equation 3 was applied to the high-angle tail of the SAXS patterns (0.18−0.35 nm^{-1}) to monitor the temperature-dependent deviations from the classical Porod equation (see above).

3. Results

3.1. Starch Suspensions at Ambient Temperature. WAXD of waxy and regular rices, with 2% and 27% apparent amylose, respectively, displayed A-type powder diffraction patterns typical for cereal starches.[27] The potato starch specimen (14% apparent amylose) showed the B-type diffraction pattern (Figure 1). SAXS patterns of starch suspensions at ambient temperature exhibited characteristic scattering maxima at $s = 0.107$, 0.103, and 0.107 nm^{-1} for the waxy rice, regular rice, and potato starch samples, respectively (Figure 2). SAXS patterns of hydrated starches have often been interpreted in terms of the paracrystalline one-dimensional lamellar stack model.[28] The upturn at the small-angle side of the first-order peak results partially from

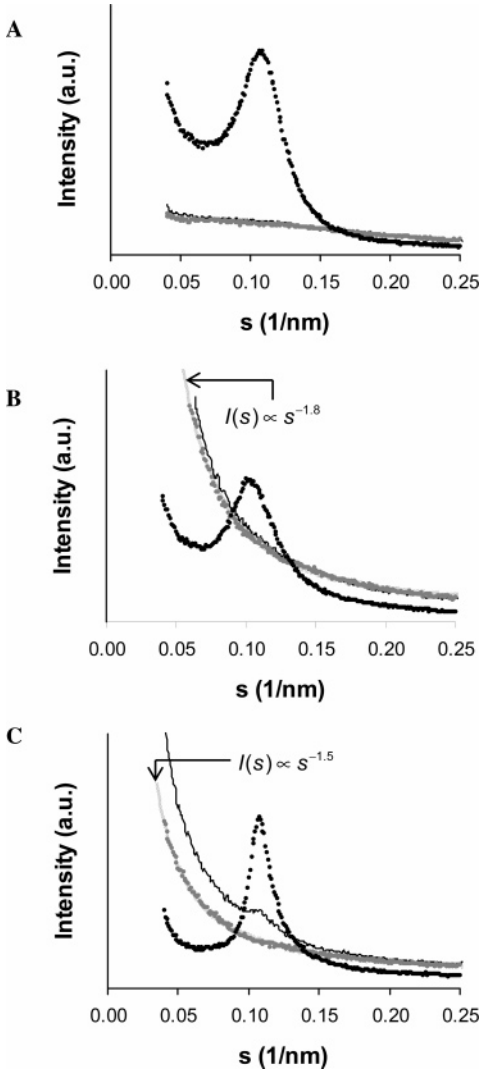

Figure 2. Small-angle X-ray scattering patterns of waxy rice starch (A), regular rice starch (B), and potato starch (C) suspensions at 30 (black dots) and 95 °C (grey dots). For regular rice and potato starch patterns at 95 °C, the power-law dependence of the scattering is visualized. Scattering patterns at DSC endpoints of gelatinization (T_{end}) are indicated with a continuous black line.

the presence of a third phase (amorphous growth ring), while the first-order and higher order scattering maxima, if present, are mainly determined by the structure of the alternating amorphous and crystalline lamellae. The contribution of the third phase to the main scattering peak becomes negligible when (i) its dimension largely exceeds those of the individual lamellae[26,29] and (ii) its density is not too different from the average density in the lamellar stack.[30] As both conditions are fulfilled in granular starches,[31,32] the two-phase approximation, and hence the use of correlation function analysis, is justified. From the correlation functions it was inferred that the lamellar repeat distance and fractional lamellar crystallinities of the starches were similar: $D = 8.8$ nm, $\varphi = 0.65$ for the waxy rice starch; $D = 8.9$ nm, $\varphi = 0.75$ for the regular rice starch; $D = 8.8$ nm, $\varphi = 0.68$ for the potato starch. Results are in broad agreement with literature data.[33] In ideal systems (i.e., structures with sharp phase boundaries between the lamellae), $D\varphi$ corresponds to the average dimension of the crystalline lamella. When transition layers are present, $D\varphi$ corresponds to the average thickness of the high-density core of the crystalline lamella added to the thickness of one transition layer. For the samples examined in this study $D\varphi$ ranged from 5.7 to 6.7 nm. The literature indicates that extensive acid hydrolysis of starches yields a bimodal dextrin population. The smallest dextrins have modal degrees of polymerization ranging from 13 (for A-type starches) to 15 (for B-type starches) and correspond to amylopectin chains spanning the high-density regions in the native starches.[6,7] As the 'length' of a single glucose monomer in crystalline conformation is 0.35 nm,[8] the high-density cores of crystalline lamellae measure 4.6−5.3 nm. Comparison of these estimates with the dimensions of the thickness of the crystalline lamellae obtained from SAXS analyses suggests that lamellae are delimited by transition layers of about 0.7−2.1 nm. Theoretically, transition layer dimensions can be estimated from eq 1. However, crystal edges, which are present when individual crystallites in the dense lamellae have finite lateral dimensions,[34] and anisotropic density fluctuations within the phases[35] additionally impact the high-angle tail of SAXS patterns without affecting the central region of the scattering pattern where the first-order 9 nm scattering feature of stacked lamellae is dominant. In view of the limited lateral dimensions of amylopectin crystallites (7−14 nm)[2,36,37] and the presence of amylopectin branching points in the crystalline lamellae,[6] no reliable quantitative estimates on transition layer thickness can be obtained from starch SAXS patterns.

As the Porod equation describes the scattering of surface fractals ($I(s) \propto s^{-d}$ with $d = 4$), it is considered that granular starches exhibit surface fractal scattering behavior in the high s range.[38] The presence of transition layers results in $d > 4$ when SAXS patterns are analyzed in terms of fractals with eq 3. Corresponding data are, however, not strictly linear in a double-logarithmic plot, as is obvious from eq 1. Although the fractal concept is artificial here, the d values obtained, however, are valuable in following structural changes as discussed in section 3.3.

3.2. Fully Gelatinized Starch Pastes. From the WAXD patterns of gelatinized starches it is evident that all samples were fully amorphous at 95 °C (Figure 1). In line with results on gelatinized maize and potato starches[38] and amylose gels,[39] the SAXS patterns of fully gelatinized regular starches displayed power-law behavior over the full angular range (Figure 2; $I(s) \propto s^{-d}$ with $s = 0.04-0.35$ nm^{-1}). Exponents for the potato and regular rice starches ($d = 1.5$ and 1.8, respectively) are slightly lower than the values reported in the literature ($d = 1.7-2.1$).[38,39] Power-law dependence of SAXS may indicate the presence of fractal structures, and electron microscopy of quenched amylose solutions accordingly revealed self-similar structures.[40] For the gelatinized waxy maize starch, only a very weak pattern remained at 95 °C (Figure 2), which is indicative of a nearly homogeneous amylopectin solution. At this stage it is tempting to link the above to macroscopic rheological properties of gelatinized starch dispersions. Regular starches, with a more pronounced fractal structure, develop into firmer gels than waxy starches.[41] While in the high-angle tail (0.18−0.35 nm^{-1}) the scattering of waxy rice paste was adequately described by $I(s) \propto s^{-1.9}$ (see below), the power-law scattering behavior was not extended to smaller angles. As power-law scattering extends to $s > 1/R$, with R being the dimension of the fractal cluster,[39] this indicates that fractals, if present, have smaller dimensions in waxy maize pastes ($R < 6$ nm) than in amylose-containing gels ($R > 25$ nm).[39]

In contrast to the scattering behavior of granular starches, which indicates surface-fractal structures, starch pastes display power-law exponents $d < 3$, indicative of mass fractals. In the next section the transition from one type of structure to the other, i.e., the starch gelatinization process, is discussed.

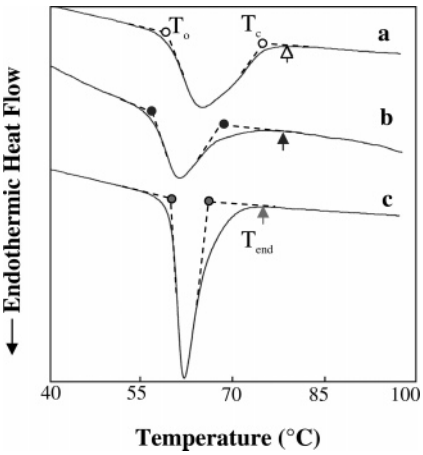

Figure 3. DSC traces of waxy rice (a), regular rice (b), and potato (c) starch suspensions. DSC onset (T_o) and conclusion (T_c) temperatures of gelatinization are indicated by circles. The end of the gelatinization endotherm (T_{end}) is indicated with triangles.

3.3. Starch Gelatinization. In addition to temperature-resolved SAXS and WAXD, starch gelatinization was also examined with fast ramp DSC, which has become the method of reference in the past decades. DSC traces with relevant parameters are displayed in Figure 3.

High-Angle Tail of SAXS Patterns. The fractal-like scattering behavior in the high-angle tail of the SAXS patterns was evaluated by fitting eq 3 in the angular range $0.18 < s < 0.35$ nm^{-1}. Figure 4A shows typical high-angle SAXS patterns of granular (30 °C) and fully gelatinized (95 °C) potato starches as well as patterns at DSC onset and conclusion temperatures. Not only did the high-angle intensity increase markedly during gelatinization, but the angular dependence changed as well. The temperature dependence of the latter was monitored for the three starch samples in Figure 4B. At ambient temperature, power-law exponents were in the range $4 < d < 5$, which is in fair agreement with $d = 4$ expected for the Porod region of structures with sharp phase boundaries (i.e., surface fractals) and deviations from transition regions. The power-law exponents remain constant up to the DSC onset temperature of gelatinization. This suggests that the surface structures within starch granules are not affected at subgelatinization temperatures. The main scattering features are hence dominated by the alternating crystalline and amorphous lamellae recognized by electron microscopy.[4] The use of (three- or two-phase) one-dimensional paracrystalline models to assess structural information in this temperature range thus seems justified.

Increasing deviations from $d = 4$ in the DSC gelatinization range indicate that the molten crystallites and lamellae do not instantaneously form homogeneous melts or solutions. From the scattering profiles of fully gelatinized starches (see above), it is deduced that amylose organizes into fractal-like structures that withstand dissolution at high temperatures. As the molecular mobility of the amylose increases during gelatinization and starch gelatinization is a granule per granule event,[3] it is plausible that network formation is effectively initiated at temperatures as low as the DSC onset of gelatinization. At 95 °C, waxy rice starch behaves essentially as an amylopectin solution. It cannot be excluded, however, that transient structures of amorphous amylopectin (i.e., granular remnants) can substantially contribute in the small-angle scattering of incompletely gelatinized starch systems. Analysis of the high-angle tail of SAXS patterns thus indicates that gelatinization is more than a simple melting of lamellar crystallites. Moreover, formation of fractal-like structures during gelatinization makes the quantitative interpretation of SAXS data in terms of the paracrystalline lamellar model rather difficult.

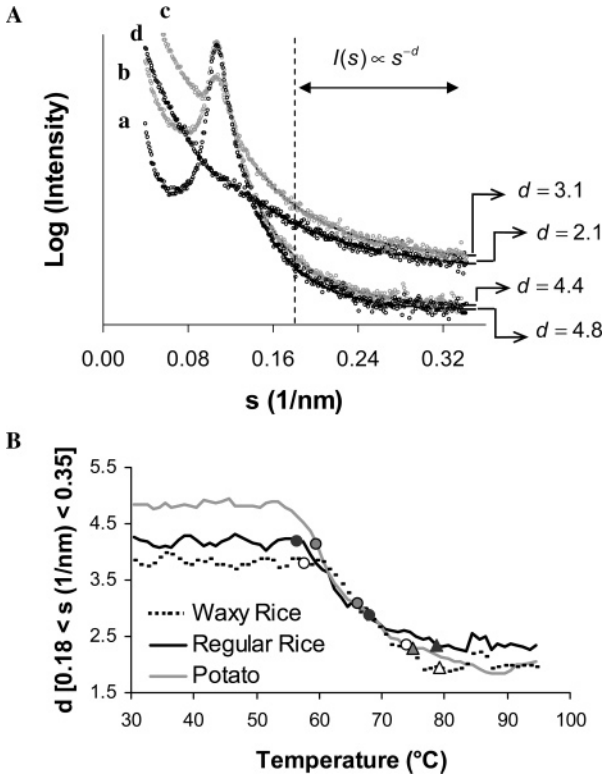

Figure 4. Power-law scattering in the high-angle tail ($I(s) \propto s^{-d}$ with $0.18 < s < 0.35$ nm^{-1}) of potato starch suspensions (A) at 30 °C (a), DSC onset temperature of gelatinization (T_o) (b), DSC conclusion temperature of gelatinization (T_c) (c), and 95 °C (d). Temperature dependence of power-law exponent (B) of waxy rice, regular rice, and potato starch. T_o and T_c of the respective starches are indicated with circles. The end of the gelatinization endotherm (T_{end}) is indicated with triangles.

Central Region of SAXS Patterns. Figure 5 depicts temperature-resolved SAXS ($0.03 < s < 0.25$ nm^{-1}) of starch suspensions. Heating suspensions to T_o did not influence the intensity of the first side maximum in the scattering pattern of waxy rice starch, while a substantial increase was observed for the regular rice and potato starches.

The total scattering power of the stacked lamellae evolved similarly, as indicated by Q_{id}, obtained from linear correlation functions (Figure 6). It is worth noting that starch annealing, the prolonged heating of starch below its gelatinization temperature in excess water, showed similar effects.[42,43] Neither D nor φ changed during fast ramp heating at subgelatinization temperatures, indicating that, on average, the lamellar structures were unaffected. Theoretically, the invariant of an ideal two-phase system is proportional to

$$Q_{id} \propto \alpha_s \varphi(1 - \varphi)(\Delta\rho_i)^2 \quad (4)$$

with α_s being the volume fraction of the lamellar stacks and $\Delta\rho_i$ the electron density difference between the amorphous and crystalline lamellae.[26] As α_s at most slightly decreases due to limited and reversible swelling of the amorphous growth rings[3] and φ remains constant, the pronounced increase of Q_{id} for the regular rice and potato starches can only be caused by a more pronounced density contrast between amorphous and crystalline lamellae. It is appealing to relate the above phenomenon to amylose diffusion within the semicrystalline growth rings. However, in doing so differences in amylopectin structure and,

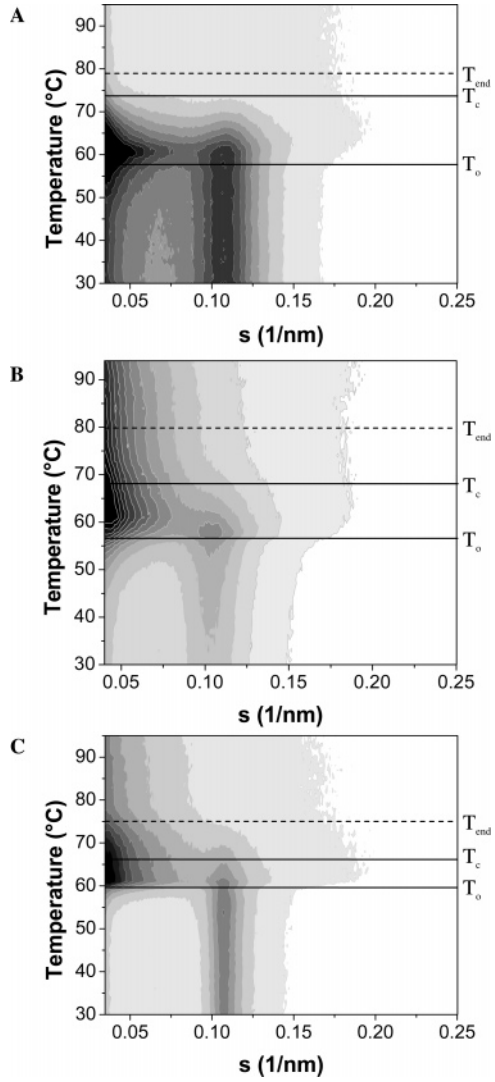

Figure 5. Temperature-resolved SAXS patterns of waxy rice starch (A), regular rice starch (B), and potato starch (C) suspensions (66% moisture). Darker colors correspond to higher intensities. DSC onset (T_o), conclusion (T_c), and end temperatures (T_{end}) are indicated by horizontal lines.

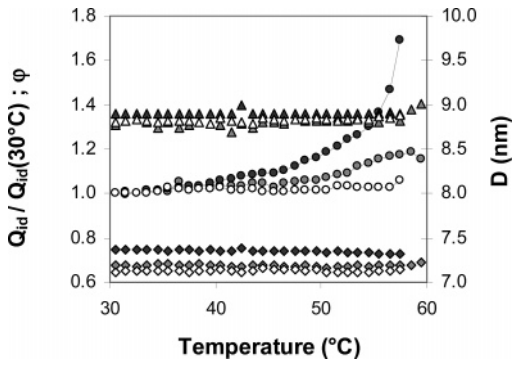

Figure 6. Lamellar repeat distance (D, triangles), fractional lamellar crystallinity (φ, squares), and invariant (Q_{id} normalized to Q_{id} at 30 °C, circles) of waxy rice starch (open symbols), regular rice starch (black symbols), and potato starch (grey symbols) suspensions (66% moisture) up to the DSC onset temperatures of the respective samples.

consequently, liquid-crystalline properties are neglected. For all starches the intensity at the smallest angles ($s < 0.07$ nm^{-1}) already increased at subgelatinization temperatures. According to the three-phase paracrystalline model, this relates to an increased electron density difference between the amorphous growth ring and the amorphous lamellae in the semicrystalline growth ring. An influx of water in the amorphous growth ring can trigger such increased density contrast.[28]

Within the DSC-gelatinization temperature range, SAXS patterns of starches are characterized by (i) an initial further increase of the intensity at very low angles ($s < 0.07$ nm^{-1}) and (ii) a decrease of the first-order scattering peak intensity. Within the framework of the three-phase paracrystalline model, the former has been ascribed to a higher contrast between the amorphous and semicrystalline growth rings.[10] Although this interpretation is in line with findings at subgelatinization temperatures (see above), the use of paracrystalline models to obtain quantitative structural data on gelatinizing starches is limited because of (i) the development of mass fractals and (ii) the possible fragmentation of large superstructures. For amylose-containing starches, self-similar amylose structures are anticipated to contribute appreciably to the observed scattering patterns. Furthermore, during gelatinization growth rings may break up. The decreasing dimensions of the resulting transient structures would shift the corresponding scattering to larger angles, leading to an increased scattering in the experimentally accessible window. The breakdown of semicrystalline growth rings and the improved contrast between amorphous and semicrystalline growth rings[28] can thus both explain the increased intensity at the high-angle side of the 9 nm scattering maximum of waxy and regular starches during the initial stages of gelatinization.

The decrease in the first-order scattering peak during gelatinization was interpreted in terms of the invariant and probably results from a reduction of the volume fraction of stacked lamellae (α_s in eq 4).[42]

The temperature dependence of the intensity increment at very low angles and the decrease of the 9 nm scattering maximum are markedly different for the various starches. The first-order scattering peak of waxy rice starch collapsed around 60 °C, some 2−3 °C above T_o. Concurrently, the low-angle scattering $s < 0.07$ nm^{-1} rapidly decreased until only a very weak pattern remained at 80 °C. Compared to the waxy starch, the first-order scattering peak of the regular rice starch decayed at lower temperatures relative to the respective T_o. This concurs with the results of Donald and co-workers,[44] who suggested that amylose diffuses into the amylopectin crystalline lamellae and disturbs lamellar organization. Upon gelatinization the regular rice starch developed a more pronounced low-angle scattering which was less influenced by temperature than the scattering of the waxy rice starch paste (Figure 5). The scattered intensity remained high throughout the gelatinization range, suggesting that amylose is involved in the formation of a stable self-similar network in the gelatinized starch paste. The first-order scattering peak of potato starch drastically decreased above T_o. The intensity at the smallest angles increased further, however, and only beyond T_p (61.9 °C) did the scattering decrease. In contrast to the other starches, a weak trace of the first-order maximum remained up to T_{end} (Figures 2 and 5). Temperature-resolved WAXD (see below) confirms the presence of residual structural order at the end of the potato starch gelatinization endotherm.

Temperature-Resolved WAXD. Although DSC traces (Figure 3) of the waxy rice and potato starches differed markedly, the temperature dependence of their CI was quite similar (Figure 7). For the waxy rice starch the loss of crystallinity coincided with the DSC gelatinization endotherm with CI < 0.10 at T_c. The regular rice starch showed a somewhat higher residual crystallinity (CI 0.17 at T_c). The observed value falls within

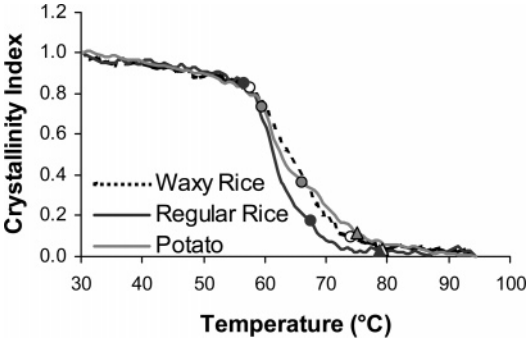

Figure 7. Temperature dependence of WAXD crystallinity of waxy rice, regular rice, and potato starch suspensions. DSC onset (T_o) and conclusion (T_c) temperatures are indicated with circles. The end of the gelatinization endotherm (T_{end}) is indicated with triangles.

the range ($0.15 < CI < 0.22$) found for a wider set of regular rice starches (unpublished results). For potato starch CI exceeded 0.30 at T_c (Figure 7). Even when the high-temperature tail of the rather asymmetric endotherms was taken into account (T_{end} in Figure 2), residual crystallinity was higher for potato than for waxy rice starch. Residual crystallinity at the end of the gelatinization endotherm has been observed earlier[10] and was ascribed to small and imperfectly organized crystallites or individual double helices. Recently, however, the starch gelatinization endotherm was reported to be followed by an exothermic process resulting from free ends of unwound amylopectin double helices associating with other amylopectin branch chains to form an amorphous hydrogen-bonded network.[15,16] Exothermic events partially overlapping with the end of the endothermic transition may result in deceivingly low DSC T_c values. In addition to residual crystallinity (WAXD), SAXS indicated some residual lamellar organization at the end of the gelatinization endotherm for potato starch. Fast exothermic reassociations of amylopectin are hence thought to overlap with the endothermic gelatinization event. The literature indeed shows that potato amylopectin, which has longer outer branches than amylopectins of A-type starches, retrogrades more readily.[45] Moreover, SAXS suggests the formation of self-similar amylose structures, which should be accompanied by an exothermic process. As WAXD revealed systematic higher crystallinities at T_c for regular than for waxy starches, a plausible role of amylose in the formation of hydrogen-bonded networks is indeed envisaged. [46−48]

Differences in rate of network formation and network-forming capacity can be anticipated for amylose and different amylopectins, and the resulting diverse exothermic events at the high-temperature side of the gelatinization endotherm may lead to inaccuracies in the determination of T_c.

4. Conclusions

The angular dependence of the X-ray scattering in the high-angle region of SAXS patterns ($0.18 < s < 0.35$ nm^{-1}) changed markedly at temperatures corresponding to the DSC gelatinization range. Irrespective of the amylose content and the crystal type of the granular starch, the power-law scattering behavior evolved with a decrease of the exponent from approximately 4 to 2. At 95 °C, the power-law scattering behavior extended, however, to lower scattering angles ($s = 0.04$ nm^{-1}) for the amylose-containing starches, indicating that amylose is essential in the development of large, temperature-stable self-similar structures. In partially gelatinized systems, the simultaneous presence of fractal-like structures and residual lamellar stacks largely complicates SAXS pattern analysis in terms of the classical paracrystalline models.

Although regular A-type starch had a slightly higher crystallinty index at the DSC endpoint of gelatinization than the waxy starch, the temperature range of crystal melting corresponded roughly to the DSC gelatinization range. WAXD indicated, however, residual crystallinity for B-type starch at the end of the gelatinization endotherm, while its SAXS patterns still displayed the 9 nm repeat. It is suggested that formation of an amorphous network by reassociations of amylose and the outer branches of amylopectin gives an exothermic contribution to the DSC trace. Results indicate that, during gelatinization, endothermic amylopectin crystal melting is accompanied by the exothermic formation of amorphous networks. Involvement of amylose adds to the thermal stability of the latter structure. Along with the larger dimensions of the corresponding fractal structures, the latter might explain why amylose-containing starches develop into firm macroscopic gels while the gel-forming capacity of waxy starches is much less pronounced.

Abbreviations Used

CI, crystallinity index; D, lamellar repeat distance; DSC, differential scanning calorimetry; MW, weight-average molecular weight; Q_{id}, the invariant; SAXS, small-angle X-ray scattering; SCLCP, side-chain liquid-crystalline polymer; T_o, DSC onset temperature of gelatinization; T_p, DSC peak temperature; T_c, DSC conclusion temperature; T_{end}, DSC end temperature; WAXD, wide-angle X-ray diffraction.

Acknowledgment. R.V. acknowledges the 'Instituut voor de Aanmoediging van Innovatie door Wetenschap en Technologie in Vlaanderen' (IWT, Brussels, Belgium) for the receipt of a scholarship. B.G. is a postdoctoral fellow of the 'Fonds voor Wetenschappelijk Onderzoek-Vlaanderen' (FWO-Flanders, Brussels, Belgium). B.G., H.R., and J.A.D. thank the FWO−Flanders for continuous support and equipment. Technical assistance by Dr. E. Theunissen (Laboratory of Macromolecular Structural Chemistry, K. U. Leuven) and Dr. G. Vandeputte and Luc Van den Ende (Laboratory of Food Chemistry, K. U. Leuven) is gratefully appreciated.

References and Notes

(1) Yoo, S. H.; Jane, J. *Carbohydr. Polym.* **2002**, *49*, 307−314.
(2) Hizukuri, S. In *Carbohydrates in Food*; Eliasson, A. C., Ed.; Marcel Dekker: New York, 1996; pp 347−429.
(3) French, D. In *Starch Chemistry and Technology*; Whistler, R. L., BeMiller, J. N., Paschall, J. F., Eds.; Academic Press: San Diego, CA, 1984; pp 183−247.
(4) Oostergetel, G. T.; van Bruggen, E. F. J. *Starch/Stärke* **1989**, *41*, 331−335.
(5) Waigh, T. A.; Perry, P.; Riekel, C.; Gidley, M. J.; Donald, A. M. *Macromolecules* **1998**, *31*, 7980−7984.
(6) Jane, J. L.; Wong, K. S.; McPherson, A. E. *Carbohydr. Res.* **1997**, *300*, 219−227.
(7) Vermeylen, R.; Goderis, B.; Reynaers, H.; Delcour, J. A. *Biomacromolecules* **2004**, *5*, 1775−1786.
(8) Imberty, A.; Buléon, A.; Tran, V.; Pérez, S. *Starch/Stärke* **1991**, *43*, 375−384.
(9) Waigh, T. A.; Gidley, M. J.; Komanshek, B. U.; Donald, A. M. *Carbohydr. Res.* **2000**, *328*, 165−176.
(10) Jenkins, P. J.; Donald, A. M. *Carbohydr. Res.* **1998**, *308*, 133−147.
(11) Atkin, N. J.; Abeysekera, R. M.; Cheng, S. L.; Robards, A. W. *Carbohydr. Polym.* **1998**, *36*, 173−192.
(12) Atwell, W. A.; Hood, L. F.; Lineback, D. R.; Varriano-Marston, E.; Zobel, H. F. *Cereal Foods World* **1988**, *33*, 306−311.
(13) Liu, H.; Lelièvre, J.; Ayoung-Chee, W. *Carbohydr. Res.* **1991**, *210*, 79−87.
(14) Cooke, D.; Gidley, M. J. *Carbohydr. Res.* **1992**, *227*, 103−112.

(15) Randzio, S. L.; Flis-Kabulska, I.; Grolier, J. P. E. *Macromolecules* **2002**, *35*, 8852−8859.
(16) Randzio, S. L.; Orlowska, M. *Biomacromolecules* **2005**, *35*, 3045−3050.
(17) Morrison, W. R.; Milligan, T. P.; Azudin, M. N. *J. Cereal Sci.* **1984**, *2*, 257−271.
(18) Vandeputte, G. E.; Vermeylen, R.; Geeroms, J.; Delcour, J. A. *J. Cereal Sci.* **2003**, *38*, 43−52.
(19) °C = K − 273.15 with Kelvin (K) being the basic SI temperature unit.
(20) Chrastil, J. *Carbohydr. Res.* **1987**, *159*, 154−158.
(21) Rapp, G.; Gabriel, A.; Dosière, M.; Koch, M. H. J. *Nucl. Instrum. Methods* **1995**, *A357*, 178−182.
(22) Vermeylen, R.; Derycke, V.; Delcour, J. A. Goderis, B.; Reynaers, H.; Koch, M. H. J. *Biomacromolecules* **2006**, *7*, 1231−1238.
(23) Boulin, C.; Kempf, R.; Koch, M. H. J.; McLaughlin, S. M. *Nucl. Instrum. Methods* **1986**, *A249*, 399−407.
(24) Derycke, V.; Vandeputte, G. E.; Vermeylen, R.; De Man, W.; Goderis, B.; Koch, M. H. J.; Delcour, J. A. *J. Cereal Sci.* **2005**, *42*, 334−343.
(25) Stribeck, N.; Alamo, R. G.; Mandelkern, L.; Zachmann, H. G. *Macromolecules* **1995**, *28*, 5029−5036.
(26) Goderis, B.; Reynaers, H.; Koch, M. H. J.; Mathot, V. B. F. *J. Polym. Sci., B: Polym. Phys.* **1999**, *37*, 1715−1738.
(27) Buléon, A.; Colonna, P.; Planchot, V.; Ball, S. *Int. J. Biol. Macromol.* **1998**, *23*, 85−112.
(28) Cameron, R. E.; Donald, A. M. *Polymer* **1992**, *33*, 2628−2636.
(29) Crist, B. *J. Macromol. Sci.-Phys.* **2000**, *B39*, 493−518.
(30) Wenig, W.; Brämer, R. *Colloid Polymer Sci.* **1978**, *256*, 125−132.
(31) Jenkins, P. J.; Donald, A. M. *Int. J. Biol. Macromol.* **1995**, *17*, 315−321.
(32) Daniels, D. R.; Donald, A. M. *Biopolymers* **2003**, *69*, 165−175.
(33) Perry, P. A.; Donald, A. M. *Biomacromolecules* **2000**, *1*, 424−432.
(34) Albrecht, T.; Strobl, G. *Macromolecules* **1995**, *28*, 5267−5273.
(35) Ruland W. *J. Appl. Crystallogr.* **1971**, *4*, 70−73.
(36) Jenkins, P. J.; Donald, A. M. *J. Appl. Polym. Sci.* **1997**, *66*, 225−232.
(37) Väänänen, T.; Ikonen, T.; Jokela, K.; Serimaa, R.; Pietilä, L.; Pehu, E. *Carbohydr. Polym.* **2003**, *54*, 499−507.
(38) Suzuki, T.; Chiba, A.; Yano, T. *Carbohydr. Polym.* **1997**, *34*, 357−363.
(39) Vallêra, A. M.; Cruz, M. M.; Ring, S.; Boué, F. *J. Phys.: Condens. Matter* **1994**, *6*, 311−320.
(40) Putaux, J. L.; Buléon, A.; Chanzy, H. *Macromolecules* **2000**, *33*, 6416−6422.
(41) Ortega-Ojeda, F. E.; Larsson, H.; Eliasson, A. C. *Carbohydr. Polym.* **2004**, *57*, 55−66.
(42) Jacobs, H.; Mischenko, S.; Koch, M. H. J.; Eerlingen, R. C.; Delcour, J. A.; Reynaers, H. *Carbohydr. Res.* **1998**, *306*, 1−10.
(43) Vermeylen, R.; Goderis, B.; Delcour, J. A. *Carbohydr. Polym.* **2006**, *14*, 364−375.
(44) Donald, A. M.; Kato, K. L.; Perry, P. A.; Waigh, T. A. *Starch/Staerke* **2001**, *53*, 504−512.
(45) Frederiksson, H.; Silverio, J.; Andersson, R.; Eliasson, A. C.; Åman, P. *Carbohydr. Polym.* **1998**, *35*, 119−134.
(46) Le Lay, P.; Delmas, G. *Carbohydr. Polym.* **1998**, *37*, 49−60.
(47) Bernazzani, B.; Chapados, C.; Delmas, G. *J. Polym. Sci., B: Polym. Phys.* **2000**, *38*, 1662−1677.
(48) Bernazzani, B.; Chapados, C.; Delmas, G. *Biopolymers* **2001**, *58*, 305−318.

BM060252D